Integrated Ultra-Low-Loss 4-Bit Tunable Delay for Broadband Phased Array Antenna Applications

Renan L. Moreira, John Garcia, Wenzao Li, Jared Bauters, Jonathon S. Barton, Martijn J. R. Heck, John E. Bowers, and Daniel J. Blumenthal

***Abstract*— We demonstrate the design, fabrication, and characterization of a 4-bit tunable delay in an ultra-low-loss Si_3N_4 planar platform. Temporal delays up to 12.35 ns with resolution of 0.85 ns are measured, for a total of 2.407 meters of propagation length. The TE waveguide propagation loss is measured to be (1.01 ± 0.06) dB/m at a wavelength of 1550 nm with the lowest loss of (0.57 ± 0.08) dB/m at 1591 nm.**

***Index Terms*— Optical waveguides, planar lightwave circuit, optical delay.**

I. Introduction

OPTICAL true time delays (TTD) could be a great solution for broadband phased array antenna applications in order to reduce beam-squint, i.e., beam deformation due to frequency change, and electromagnetic interference [1]. TTD for large aperture antennas and arrays with a high number of elements require delay lengths in the tens of nanosecond scale. Several fiber based optical TTD have been demonstrated [2], [3] at much longer range, which are attractive due to their low propagation loss but suffer from the fact that they are bulky and must have their length precisely cleaved in order to achieve accurate delays. As a result, integration of such devices would benefit the system by decreasing the footprint, increasing the delay accuracy, increasing stability and reducing cost. Although many fully integrated optical TTD have been demonstrated [4]–[7], the maximum amount of delay is usually limited by high propagation loss limiting the delay time to the picosecond range or a few nanoseconds. We have recently demonstrated record low propagation losses in a Si_3N_4/SiO_2 planar waveguide technology, which allows for long delays to be implemented on chip scale devices [8], [9].

In this letter, we present the fabrication of the longest fully integrated 4-bit true time delay on the ultra-low-loss planar Si_3N_4/SiO_2 platform with delays up to 12.35 ns. The device presented here is also easily scalable for even longer delay lines and higher bit count delays given the low propagation loss of the platform.

Manuscript received January 30, 2013; revised March 18, 2013; accepted April 26, 2013. Date of publication May 6, 2013; date of current version May 30, 2013. This work was supported in part by DARPA MTO under the iPhod Project under Contract HR0011-09-C-0123.

The authors are with the Department of Electrical and Computer Engineering, University of California, Santa Barbara, CA 93106 USA (e-mail: rmoreira@ece.ucsb.edu; johngarcia@ece.ucsb.edu; wli@ece.ucsb.edu; jbauters@ece.ucsb.edu; jsbarton@ece.ucsb.edu; mheck@ece.ucsb.edu; bowers@ece.ucsb.edu; danb@ece.ucsb.edu).

Color versions of one or more of the figures in this letter are available online at http://ieeexplore.ieee.org.

Digital Object Identifier 10.1109/LPT.2013.2261807

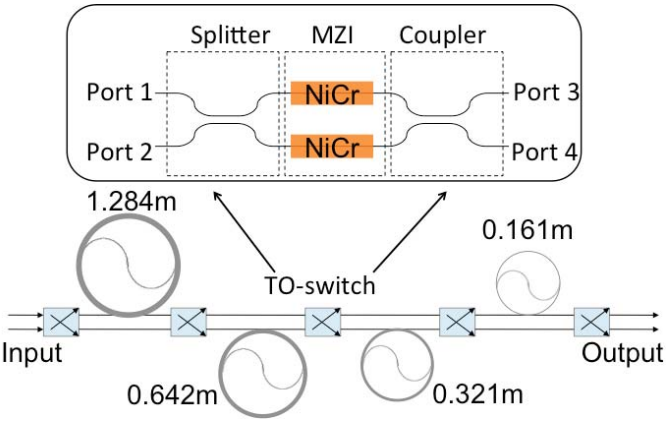

Fig. 1. Schematic of the tunable delay with the respective delay length for each stage. Inset: Thermo-optic switch schematic.

II. Design and Fabrication

The 4-bit tunable delay consists of four delay elements and five thermo-optic switches (TO-switches), and was designed according to the schematic shown in Figure 1. The TO-switches were based on Mach-Zehnder interferometers, as seen in the inset of Figure 1. Nickel Chrome (NiCr) was used as the heating element due to its high sheet resistance.

The device was physically laid out according to the mask layout as shown in Figure 2a where each delay is routed to its appropriate switch accordingly, and was designed to have lengths of 1.284 m, 0.642 m, 0.321 m, and 0.161 m, where each delay is half of the previous delay, i.e. τ, $\tau/2$, $\tau/4$, $\tau/8$. A total of 16 different delays may be selected by choosing from an individual delay or a combination of delay elements. The device therefore provides nominal delays from 0 to 12.00 ns, with respect to the minimum path length, for a maximum total of 2.407 meters in propagation length and a simulated group index of 1.49.

The waveguide geometry used for the device was based on the low loss silicon nitride platform reported in [9]. The waveguide cross section can be seen in Figure 2b. The device was fabricated on a 100 mm Silicon substrate with 15 μm of thermal oxide as the lower cladding (n = 1.45), with a core waveguide thickness of 60 nm of stoichiometric Si_3N_4 (n = 1.98) deposited by low-pressure chemical vapor deposition (LPCVD) and patterned by contact lithography. The upper cladding consisted of 3 μm of SiO_2 deposited by tetraethylorthosilicate (TEOS) based LPCVD, and 3 additional

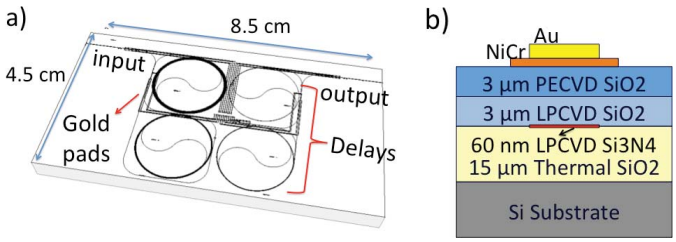

Fig. 2. a) Actual mask layout of the device displaying the position of each delay elements. The diced out device has a dimension of 4.5 cm × 8.5 cm. b) Waveguide cross-section.

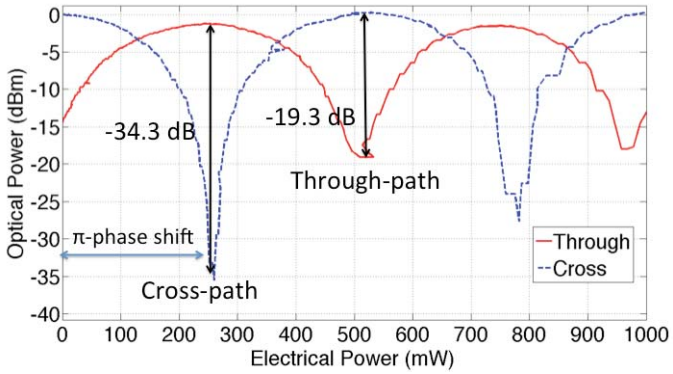

Fig. 3. Measured switch optical output as a function of switch bias at an operating temperature of 36 °C in order to compensate for fabrication variances.

micrometers of high-density plasma enhanced chemical vapor deposition (HD-PECVD) SiO_2. The heating elements for the TO-switches were realized by depositing 8 total alternating layers of Nickel and Chrome of thickness of 12.5 nm and 6.0 nm, respectively. The NiCr was deposited via electron-beam (e-beam) evaporation and patterned by lift-off. Finally, 1 μm of gold was then deposited as probing pads. Further details on the waveguide fabrication can be found in [8].

III. Measurements

A. Thermo-Optic Switch

The first measurement to be done was to determine the switch performance and bias point based on an identical 2×2 switch test structure. Switch speed was not measured for this experiment but is expected to be in the order of milliseconds given the thermo-optics properties of glass [10]. A 1550 nm laser was coupled into the top input of the switch and a broadband InGaAs detector at each output measured the switch response as a function of switch bias. The input polarization was optimized for maximum output power via a polarization controller.

Figure 3 shows the measured response for both outputs as a single MZI arm is biased. The data is taken as a function of switch bias and normalized to the cross path. As can be seen from the plot, the unbiased output is in the cross state. As current is applied to the NiCr heating element, the index of refraction is changed sufficiently to cause a π-phase shift allowing the output to cycle to the through path. The asymmetric isolation is a direct result of unbalanced 3-dB couplers [10]. For input into port 1, the power output can be described by the equations below:

$$T_{13} = 1 - 2\alpha(1-\alpha)(1+\cos\theta)\ [throughpath]$$
$$T_{14} = 2\alpha(1-\alpha)(1+\cos\theta)\ [crosspath] \quad (1)$$

where T_{13} and T_{14} are the switch power outputs at ports 3 and 4 for input to port 1, α is the directional couplers power-coupling ratio, and θ is the induced phase shift. As can be seen in (1), when the switch is in the cross state at $\theta = 0$, the transmission for the through path in the cross state can only reach 0 whenever the coupling ratio is exactly 50%. On the other hand, when the switch is in the through state at $\theta = \pi$, the transmittance of the cross path always reaches 0 no matter what the value of α is. As a conclusion, fabrication variations that cause the coupling ratio to be other than 3dB will always affect the extinction ratio of the through path alone. Changing the coupling constant, and essentially the coupling length to a value that corresponds to the length on the chip, via the thermo-optic effect can compensate for these fabrication variances. In order to find the optimal operating temperature for the highest switch isolation, a thermo-electric cooler was used to maintain the entire chip at a desired temperature. The temperature was varied between 22 and 38 °C, while measuring the switch isolation at each point. At room temperature, the switch had an isolation of 6.8 dB, while the best result was achieved at an operating temperature of 36 °C with a switch isolation of 19.3 dB, as seen in Figure 3. The turn-on power was also measured to be 260 mW, which corresponds to an applied average voltage of 16.0 V.

B. Optical Loss

The propagation loss of the waveguides was measured by optical frequency domain reflectometry (OFDR). Using a 1-meter spiraled waveguide test structure, the backscattered optical power was measured using a Luna OBR 4400 commercial reflectometer and the propagation loss extracted as in [8]. Figure 4 displays the TE loss as a function of wavelength for the designed waveguide. The TE loss was measured to be (1.01 ± 0.06) dB/m at 1550 nm wavelength, reaching a low-loss point of (0.57 ± 0.08) dB/m at 1591 nm. The waveguide loss displays a wavelength dependent spectrum and structures, which are a direct result of the absorption loss due to molecular bond resonances due to hydrogen impurities as seen in [8].

The total optical loss of the device was then measured at each of the 16 separate states. Each switch was biased accordingly and 0 dBm of optical power from a tunable laser at 1550 nm wavelength was coupled into the device via a cleaved single mode fiber. The optical output was then collected by another cleaved single mode fiber and detected using a broadband InGaAs detector. Figure 5 displays the measured optical loss from fiber to fiber for all 16-bit states, where State 1 represents the shortest delay in which the light travels through no delay element and State 16 is the longest delay state where the light travels through all 4 of the delay elements. All the data have been normalized to the back-to-back measurement where the chip is bypassed and the error bars are based on the standard deviation of ten

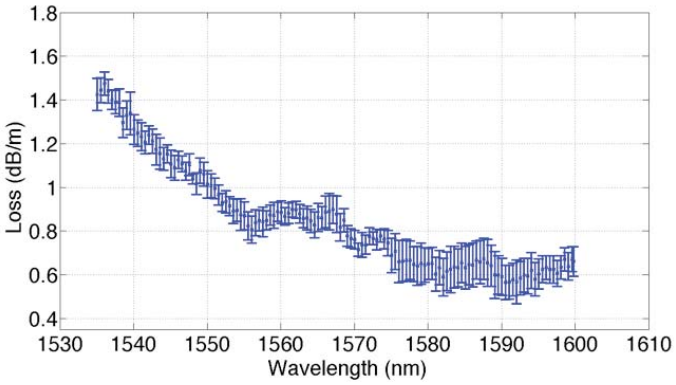

Fig. 4. Wavelength-dependent waveguide propagation loss measured via optical frequency domain reflectometry (OFDR).

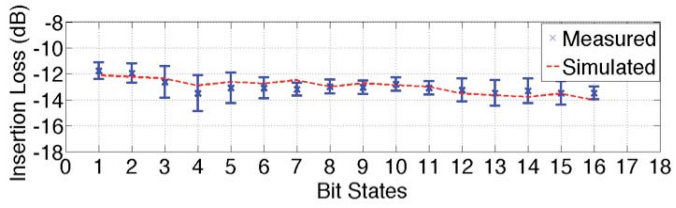

Fig. 5. Total optical loss from fiber to fiber for all 16 bit states, where state 1 is the shortest delay and 16 the longest including simulated results.

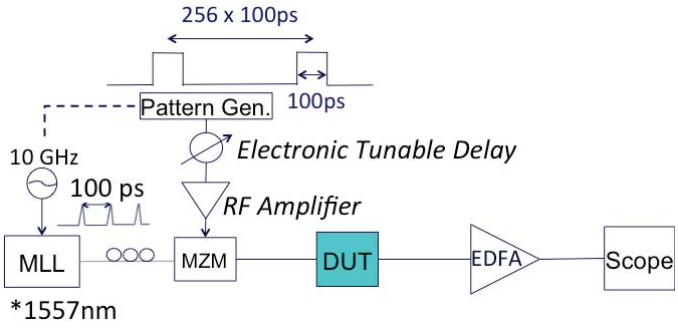

Fig. 6. Experimental set-up used to characterize delay configurations.

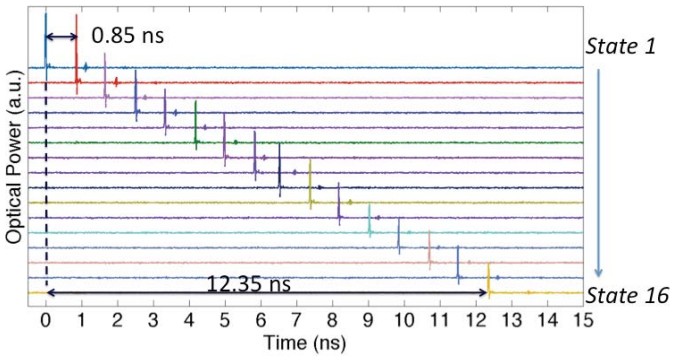

Fig. 7. Optical output of the 4-bit tunable delay for all possible delay settings.

measurements, where the variation between each measurement is caused by temperature variation as the temperature profile changes from state to state while the thermo-electric cooler (TEC) tries to maintain a constant temperature. As can be seen from Figure 5, the data display some deviation from a linear relationship from state to state, which is a result of the imbalanced switch causing the cross state to have higher loss, as shown in Fig. 3. State 4 is the only state where all the switches are set to the cross state; therefore, as can be seen in the plot, it is the state that deviates the most. The dashed line in Figure 5 is based on simulated results of 0.8 dB for loss, 1.5 dB per facet of coupling loss, and losses for the cross and through states of the switches of 1.9 and 1.7 dB, respectively.

The measurement displays a small deviation in power from state to state, which is indicative of the low-loss waveguide platform. An insertion loss (fiber-to-fiber) of 11.8 $\pm$ 0.6 dB was measured for the shortest delay and 13.5 $\pm$ 0.5 dB for the longest delay (12.35 ns).

C. Delay Measurements

Lastly, the delay measurements were collected using the experimental set-up shown in Figure 6. A mode-locked laser (MLL) centered at 1557 nm was utilized to generate a train of 2-picosecond pulses at a 10 GHz repetition rate. A pulse-carving Mach-Zehnder modulator (MZM) was used to reduce the repetition rate by a factor of 256, which was long enough to accommodate the longest delay of 12.00 ns. The polarization state was again controlled through a 3-paddle polarization controller and the light injected into the device in a transverse-electric (TE) state via a cleaved single-mode fiber. The device output signal was then collected through another cleaved single mode fiber, amplified with an Erbium-doped fiber amplifier (EDFA) at constant current, and finally sent to a sampling scope for characterization.

Figure 7 shows the optical output for the tunable delay. The plot displays the delays acquired for all 16 states of the 4-bit tunable delay with respect to the first state. The total temporal delay was measured to be 12.35 ns with a 0.85ns resolution, corresponding to a small deviation from the simulated group index due to fabrication and design.

IV. Conclusion

We demonstrated the realization of the longest fully integrated 4-bit tunable delay on an ultra-low-loss Si_3N_4 planar waveguide platform consisting of 4 delay elements and 5 thermo-optic switches. The thermo-optic switches were measured to have 19.3 dB of isolation and 260 mW of power consumption. Delays up to 12.35 ns (2.407 meters) with temporal resolution of 0.85 ns were demonstrated. Waveguide TE losses were measured to be 1.01 $\pm$ 0.06 dB/m at 1550 nm and 0.57 $\pm$ 0.08 dB/m at 1591 nm.

For the same platform we have measured coupling losses of 0.91 dB and TE losses lower than 0.1 dB/m with 50 nm cores while maintaining the critical bend radius below 5 mm [8]. In this letter, a 60 nm core and a minimum bend radius of 5 mm was used; consequently, in the future, much longer delays may be fabricated at smaller footprints.

REFERENCES

[1] I. Frigyes and A. J. Seeds, "Optically generated TTD in phase array antenna," *IEEE Trans. Microw. Theory Tech.*, vol. 43, no. 9, pp. 2378–2386, Sep. 1995.

[2] E. Ackerman, S. Wanuga, D. Kasemset, W. Minford, N. Thorsten, and J. Watson, "Integrated 6-bit photonic true-time-delay unit for lightweight 3–6 GHz radar beamformer," in *IEEE MTT-S Int. Microw. Symp. Dig.*, Jun. 1992, pp. 681–684.

[3] J. J. Lee, *et al.*, "Photonic wideband array antennas," *IEEE Trans. Antennas Propagat.*, vol. 43, no. 9, pp. 966–982, Sep. 1995.

[4] X. Wang, B. Howley, M. Chen, P. Basile, and R. Chen, "Fully-integrated 4-bit true time delay module using polymer optical switches and waveguide delay lines," in *Proc. Integr. Photon. Res. Appl./Nanophoton.*, 2006, pp. 1–3.

[5] D. S. Sumida, S. Wang, and D. M. Pepper, "Rapidly reconfigurable 8-bit chip-scale true-time-delay module for high-bandwidth-preserving, multi-aperture, free-space laser-communication transmitter," in *Proc. CLEO*, May 2005, pp. 734–736.

[6] L. Zhuang, C. G. H. Roeloffzen, R. G. Heideman, A. Borreman, A. Meijerink, and W. Etten van, "Single-chip ring resonator-based 1×8 optical beam forming network in CMOS-compatible waveguide technology," *IEEE Photon. Technol. Lett.*, vol. 19, no. 15, pp. 1130–1132, Aug. 1, 2007.

[7] S. T. Chu, *et al.*, "High index contrast photonics platform," *Proc. SPIE*, vol. 6014, pp. 110–119, Oct. 2005.

[8] J. Bauters, *et al.*, "Planar waveguides with less than 0.1 dB/m propagation loss fabricated with wafer bonding," *Opt. Express*, vol. 19, no. 24, pp. 24090–24101, 2011.

[9] J. F. Bauters, *et al.*, "Ultra-low-loss high-aspect-ratio Si3N4 waveguides," *Opt. Express*, vol. 19, no. 4, pp. 3163–3174, 2011.

[10] H. Takahashi, "Planar lightwave circuit devices for optical communication: Present and future," *Proc. SPIE*, vol. 5246, pp. 520–531, Sep. 2003.